Wearable FBG Strain Flexibility In Supplemental Oxygen-assisted Respiratory Examination

Saktioto[1*], Anisa Alya Syafri[1], Mulhida[1], Bambang Widiyatmoko[2], Dwi Hanto[2], Yan Soerbakti[1], Reeky Fardinata[1], Okfalisa[3], Dedi Irawan[4], and Rina Amelia[5]

[1] *Department of Physics, Universitas Riau, Pekanbaru 28293, Indonesia*
[2] *Research Center for Photonics, KST BJ HABIBIE, South Tangerang 15314, Indonesia*
[3] *Department of Informatics Engineering, UIN Sultan Syarif Kasim, Pekanbaru 28293, Indonesia*
[4] *Department of Physics Education, Universitas Riau, Pekanbaru 28293, Indonesia*
[5] *Department of Community Medicine, Universitas Sumatera Utara, Medan 20155, Indonesia*
[*] *Corresponding author. E-mail: saktioto@lecturer.unri.ac.id*

Received: Feb. 29, 2024; Accepted: Nov. 01, 2024

Subtle sensing is one of the important aspects required in the performance of modern medical technology, especially the detection of elusive human respiratory risks. In this regard, the fiber Bragg grating (FBG) sensor offers a high-sensitivity measurement of supplemental oxygen-assisted human respiratory characteristics through a strain approach. The FBG wavelength of 1550 nm is induced by nasal airflow and back-body surface on resting and active objects. The treated FBG will undergo deformation resulting in a change in the Bragg wavelength, which is then measured using an optical sensing interrogator and processed to obtain the strain value. The measurement results show significant FBG strain values at the micro-scale. The addition of oxygen flow in the body can increase the stretch that occurs during breathing. Therefore, the FBG sensor is more effectively used in conditions with the addition of oxygen flow.

Keywords: Fiber Bragg grating; oxygen flow; respiratory; strain

http://dx.doi.org/10.6180/jase.202511_28(11).0005

1. Introduction

Two major product revolutions namely optoelectronics and fiber optic communications have taken over the role of technology in the growth of the photonics industry over the past twenty years. In line with these developments, fiber Bragg grating (FBG) sensor technology has been developed in the opto-electro-medical sector [1]. This optical fiber has additional meaning because of its high level of precision and accuracy. FBG sensors have become one of the most studied optical components in the last decade. This FBG sensor is principally an optical strain gauge used for precise measurement of stress-induced deformation [2]. In the medical field, the measurement capability of the FBG sensor has been implemented in a device designed to monitor human body vibrations induced by diaphragmatic breathing and heart rhythm [3].

FBG shows potential advantages, such as small size, lightweight, not susceptible to electromagnetic interference, electrically neutral, and can be easily embedded into structures without affecting its mechanical properties, so that suitable and most frequently used in biomedical applications [4–6]. FBG provides many benefits with relatively few drawbacks, therefore its components are of research interest to be applied to physiological measurements [7]. FBG transmits light through the core and selectively filters out specific reflected wavelengths. When an optical fiber is given a force, the FBG will change shape resulting in a change in the Bragg wavelength [8]. This fiber is configured to ensure that light propagation is affected by the

external environment. FBG is also used to monitor physical parameters such as strain [9, 10] and temperature [11].

The strain measurement capability by FBG was adapted to monitor one of the vital signs in the human body, which is the most basic measure of the function of the human body. The four main vital signs are regularly monitored by medical professionals and healthcare providers namely body temperature [12], heart rate [13], respiration [14], and blood pressure [15]. These signs are useful for detecting or monitoring medical problems. An abnormal respiratory rate is a sensitive indicator of human respiratory problems, even in patients receiving supplemental oxygen. Respiration is an essential physiological function for living creatures in daily survival. Several fiber-optic-based sensors have been developed to monitor human respiratory conditions [16, 17]. As a sensor, FBG-type optical fiber has several advantages, namely easy to modify, relatively inexpensive, resistant to interference by electric and magnetic fields, and low power consumption [18–20]. It can detect various parameters, such as pressure [21], voltage [22], and refractive index using a lattice-based device [23].

Human respiration measurements were conducted by Defrianto et al. (2022) using optical fiber with a sinusoidal FBG bending technique with a diameter of 0.8 cm in a waist belt placed on the human respiratory diaphragm [14]. In addition, human respiration measurements using an FBG belt have also been conducted by Tavares et al. (2022) and Filosa et al. (2022) with the assistance of an optical sensing interrogator (OSI) to improve the accuracy of optical signal changes [24, 25]. Respiratory measurement through this method is carried out with the principle of FBG strain due to changes in diaphragm movement. FBG strain on the diaphragm turns out to be quite large and easily measured by the system. In fact, there is the smallest factor of respiratory circulation that turns out to store data on the diagnosis of a patient's disease, such as the subtle strain factor in the nasal airflow and back body. This is an emergency call for us to develop a subtle-sensing FBG sensor in human respiration. However, the current renewable respiratory measurement method using FBG can be updated and realized with the help of external supplements. For example, we can use oxygen supplements in measurements which can help clarify measurement readings.

This study presents the design, measurement, and analysis of the results of responses to human respiratory rhythms under two conditions. The first involves a mask over the nose with and without supplemental oxygen flow and the second consists of monitoring the respiratory response at the back-body of humans using the FBG stretch sensor. The sensor was applied to the back by analyzing the effect of positional strain (ε) on respiration in human subjects aged 21 to 24 years, using FBG with a wavelength of 1550 nm. The variations given are normal breathing conditions with and without oxygen flow and activity conditions. The data obtained is then analyzed to determine the strain value at each position.

2. Literature review

FBG is a single-mode optical fiber with periodic modulation of refractive index (n) along its core. It works on the basis of temperature and the influence of external deformations, such as strain, on the lattice structure formed by periodic variations in the refractive index changes in the optical fiber core. FBG will reflect light wavelengths that satisfy only the Bragg condition (λ_B) and transmit all others when the light passes through periodically varying high and low refractive index regions [26]. The Bragg wavelength value of FBG is shown in Eq. (1) below:

$$\lambda_B = 2n_{eff}\Lambda \tag{1}$$

where n_{eff} is the effective refractive index of the periodic structure and Λ is the periodicity of the lattice. The value of the Bragg wavelength will shift when the effective refractive index or lattice period of the FBG varies due to external disturbances such as temperature fluctuations and strain. FBG has a high sensitivity to these two parameters [27]. The strain effect on the Bragg wavelength value is defined as follows:

$$\Delta\lambda_B = \lambda_B \left[1 - \frac{{n_{eff}}^2}{2}\left[p_{12} - v\left(p_{11} + p_{12}\right)\right]\right]\varepsilon \tag{2}$$

$$\frac{\Delta\lambda_B}{\lambda_B} = \left(1 - p_\varepsilon\right)\varepsilon \tag{3}$$

where v is the Poisson's ratio, p_{11} and p_{12} are the optical strain coefficients, p_ε is the photoelastic coefficient ($p_\varepsilon \approx 0.22$), and ε is the strain value [28, 29].

Theoretically, FBG fiber optics have high efficiency and effectiveness as nanometer-scale sensors through the shift in wavelength caused by strain interactions. The wavelength will change as the periodic distance changes in distance. In addition, FBGs for strain sensing have been widely applied in almost all application areas, including condition monitoring, structural health monitoring, and fault diagnostics. The pressure applied to the FBG induces a change in the effective refractive index or lattice plane causing a shift in the wavelength. The strain sensitivity depends on the physical characteristics of the fiber such as the thermo-optical coefficient and elastic-optic properties.

It also depends on the type of strain applied, such as tension or compression [23]. The response of the wavelength variation to the FBG strain can be given by:

$$\Delta\lambda_B = \lambda_{1-}\lambda_0 \tag{4}$$

The continuity of metabolic processes in the human body is strongly influenced by breathing that occurs in the lungs through the exchange of oxygen with carbon dioxide [30]. This is also influenced by the process of inspiration which involves inhaling air through the nasal cavity or mouth from the outside environment into the lungs, as well as the process of expiration, namely exhaling air rich in carbon dioxide. An imbalance in the process of inspiration and expiration can disrupt the body's metabolic processes. Generally, the first step in identifying a patient is detecting nasal breathing and body vibration. In the past, Hikma et al. (2023) used optical fibre with a sinusoidal FBG bending technique equipped with a diameter of 0.8 cm and 1.2 cm in a waist belt that was put on the human respiratory diaphragm [17]. This allowed for the measurement of human breathing. Furthermore, Issatayeva et al. (2021) and Shi et al. (2023) have also utilised an FBG belt in order to measure human respiration. These measurements were carried out with the assistance of an OSI in order to enhance the precision of optical signal changes [31, 32]. Through the rhythm of respiratory oscillations, the FBG can detect processes with a high degree of accuracy both through the nasal airflow and vibrations on the back-body surface.

3. FBG integrated mask design

This study uses FBG optical fiber with a wavelength of 1550 nm. FBG is placed on the oxygen mask with variations in the position of the placement, namely the top as shown in Fig. 1(a), middle as shown in Fig. 1(b), and bottom as shown in Fig. 1(c). It is then set up on the oxygen mask, connected to the OSI, and functions as input and output as shown in Fig. 1(d).

Four human objects with an age range of 21 to 22 years and free from respiratory problems were measured. Untreated FBG was measured as the initial wavelength (λ_0).

Measurements are taken under normal breathing conditions by placing the object in a relaxed state without any previous physical activity as shown in Fig. 1. After that, the object is attached to the oxygen mask that has been integrated by FBG and allowed to breathe normally within 60 seconds. The second condition is breathing with an additional flow of oxygen as shown in Fig. 1(f). The flow of oxygen supplied to the object is from 1 to 10 l/min. Simultaneously, the oxygen level in the body is measured using a pulse oximeter placed on the fingertip. The result

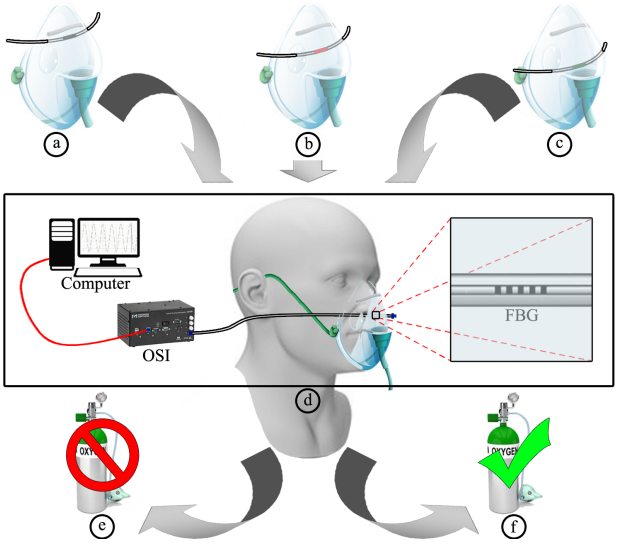

Fig. 1. The position of the FBG sensor on the mask varies, including (a) top, (b) middle, and (c) bottom. The measurement design consists of (d) the FBG inside the mask being connected to an OSI, then it is processed and forwarded to the computer by displaying output data. This sensing was carried out in a sitting position while breathing with (e) normal and (f) oxygen.

is data recorded on the monitor with a wavelength calculated by the strain value of the changes that occur in each object. The measured signal from the FBG shows the wavelength value where the strain value can be obtained from the change in wavelength using Eq. (3), then the program displays a graph of the median strain value between the maximum and minimum strain data for each FBG position in the oxygen mask. In addition, other measurements were also carried out to see which position had the highest strain value when the object was given additional oxygen at a flow range of 1 – 10 l/min. In each of these flows there is maximum, minimum, and median strain data. Furthermore, the median value was taken to be plotted to see the relationship between the strain value and oxygen flow at each position of the FBG placement on the mask.

4. FBG strain fluctuations

During normal breathing, the movement of air within the mask causes the FBG to stretch due to breathing vibrations. The values of maximum strain, minimum strain, and median are determined based on Eq. (3). Fig. 2 shows a comparison of FBG strains according to their position in the mask. These results indicate that there are significant differences in the strain values for each object. Based on the measurement results, Objects O 1 and O 2 have the

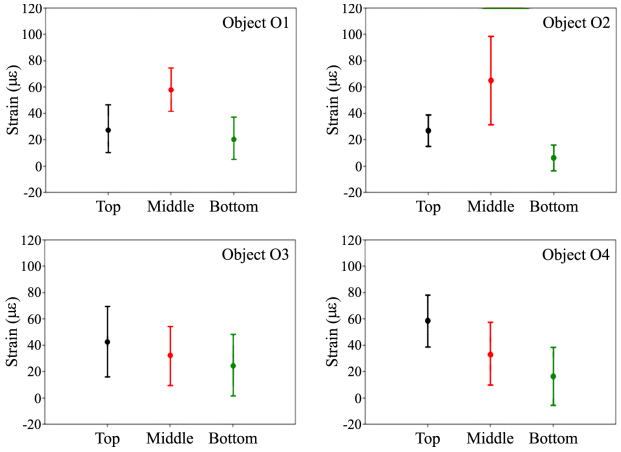

Fig. 2. FBG strain based on its position in the mask for the four objects under normal breathing conditions.

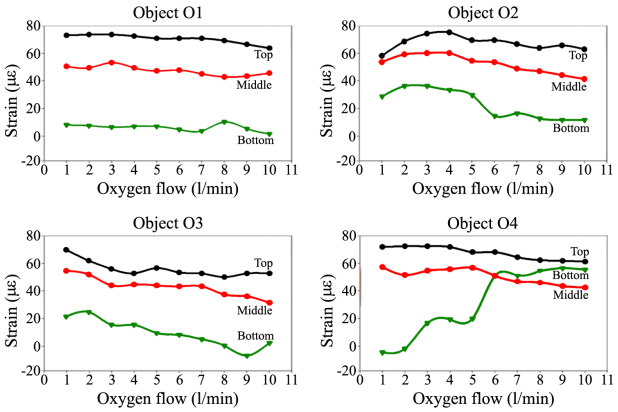

Fig. 3. The wavelength range of the FBG strain spectrum corresponds to its position in the mask under breathing conditions using supplemental oxygen for each object.

largest strain values of 57.9$\mu\varepsilon$ and 64.9$\mu\varepsilon$ in the middle position. Placing the FBG in the middle and directly in front of the nasal airflow has a greater impact on stretching the FBG than its top and bottom position with the difference between the two being approximately 37.6$\mu\varepsilon$ and 48.1$\mu\varepsilon$. Compared to objects O3 and O4, the largest FBG strain is in the upper position of 40$\mu\varepsilon$ and 60$\mu\varepsilon$. This happens because the FBG strain sensor which is placed in the top position has a large enough bend. In addition, fluctuations in the strain values on each object can occur due to shifts in the placement of the optical fiber on each object [33].

The results of measuring several FBG positions at the top, middle, and bottom of the oxygen mask as described in the methodology show that the FBG responds to changes in the wavelength value. This is caused by changes in pressure when exhaling through the nose in the oxygen mask case. Strain fluctuation conditions were obtained for the four objects after the change in wavelength was converted to strain. The sequences obtained for the four objects range from 6.2$\mu\varepsilon$ to 60$\mu\varepsilon$. These fluctuations do not show significant changes except on the order of 10^{-6}.

Breathing activity and additional flow of oxygen produce a combination of both for each experimental object. The FBG response with a wavelength function to oxygen flow is shown in Fig. 3 and Table 1. The largest FBG strain values for oxygen flow rates of 1 to 10l/min are found at the top position of each object, namely 71.9$\mu\varepsilon$ to 64.9$\mu\varepsilon$ on object $O1$, 59.6$\mu\varepsilon$ to 61.6$\mu\varepsilon$ on object O2, 70.2$\mu\varepsilon$ to 52.9$\mu\varepsilon$ on object O 3 , and 70.9$\mu\varepsilon$ to 61.9$\mu\varepsilon$ on object O 4 . All strains show a gradual decrease as oxygen flow increases. This fluctuation in strain value occurs due to the compression experienced by the FBG because both sides are being claimed to use tape. Hence, the tendency is not to expand but to experience compression [34]. The results showed that the strain value at each FBG position on the oxygen mask had a range of less than 10$\mu\varepsilon$. The fluctuations in the strain values of the four objects are caused by environmental disturbances and the sensitivity level of the nanometer-scale FBG measuring instrument. Due to the low magnitude of the noise, it is acceptable to assume that the sensitivity causes the estimates for each object to fluctuate by 10^{-6}. The change in strain decreases or increases relative to the initial state because the calculations place more emphasis on the modulus of the change in wavelength (strain).

The measured oxygen saturation values did not show a significant change from low to high flow, which was indicated by an increase of only 1% to 2%. The measurement results are shown in Table 2. These results illustrate that the object data is included in the normal category ($>$ 95%). Furthermore, normal oxygen saturation indicates good tissue perfusion, which is indicated by capillary refill time and is also supported by normal oxygen saturation [35].

5. FBG induced back-body design

Measurement of respiratory characteristics through the back-body surface is carried out by inducing the FBG attached to the tape layer. Then tested in various positions behind the adult body using OSI and a computer. An illustration of this experiment can be seen in Fig. 4(a). This test is performed while standing under normal breathing conditions and supplemental oxygen as shown in Fig. 4(b) (c). The same test was also performed while running while breathing normally and with supplemental oxygen as shown in Fig. 4(d) and (e).

The detection of breathing through the back-body surface is read by OSI as a function of the wavelength inten-

Table 1. FBG strain measurements at several positions on the mask for each object.

Oxygen flow (1/min)	Strain FBG-top ($\mu\varepsilon$)				Strain FBG-middle ($\mu\varepsilon$)				Strain FBG-bottom ($\mu\varepsilon$)			
	O1	O2	O3	O4	O1	O2	O3	O4	O1	O2	O3	O4
1	71.9	59.6	70.2	70.9	50.8	53.8	53.7	58.5	8.7	27.2	21.5	−5.2
2	72.3	70.6	63.5	71.0	49.6	59.5	51.2	49.9	8.5	36.7	24.7	−2.5
3	72.1	75.7	56.8	70.9	51.3	59.6	43.8	54.1	8.2	36.6	18.5	18.3
4	71.6	78.5	53.3	70.7	50.6	59.7	44.3	55.5	8.4	35.1	18.7	20.1
5	71.2	70.4	57.6	65.6	46.7	53.7	44.1	57.6	8.4	31.2	9.8	20.2
6	70.8	70.7	53.4	65.8	46.9	52.8	44.0	47.5	6.2	13.5	9.6	47.5
7	70.7	65.9	53.1	62.8	43.2	49.5	44.1	43.2	5.1	15.7	5.2	47.6
8	69.5	62.4	51.2	62.1	41.4	46.2	38.7	42.8	10.1	9.8	0.5	54.0
9	67.4	64.2	53.1	62.0	41.6	42.4	38.5	41.1	6.0	9.6	-9.1	57.5
10	64.9	61.6	52.9	61.9	43.3	41.2	35.2	40.2	0.2	9.5	0.9	55.1

Table 2. Measurement of oxygen saturation for each object.

Oxygen flow (1/min)	Oxygen saturation (%)			
	Object O1	Object O2	Object O3	Object O4
1	98.7	97.7	97.7	97.7
2	98.7	87.3	97.7	98.7
3	97.7	98.0	97.7	98.3
4	97.7	97.7	97.7	99.0
5	99.0	99.0	97.7	99.0
6	98.7	97.0	98.7	99.0
7	97.7	98.7	98.0	99.0
8	98.3	98.0	98.0	99.0
9	99.0	99.0	98.3	99.0
10	99.0	99.0	98.0	98.3

sity. When the laser beam passes through the FBG which is located on the back-body of a human, the FBG will feel vibrations due to inspiratory and expiratory breathing. This activity causes a shift in wavelength as a result of stretching the back body. FBG strain placement uses a non-invasive sensor that attaches directly to the back of an adult's body. The FBG reflection data is sent to the OSI connected to the monitor to display the measurement results. Then, the Bragg wavelength (λ_B), the change in Bragg wavelength ($\Delta\lambda_B$), and the strain (ε) are transformed into a function of the position of the strain ($\varepsilon = f(x)$). This calculation uses Eqs. (3) and (4) to determine the changes in Bragg wavelength and strain on the 1550 nm FBG. The data obtained from the measurement results are then programmed in the form of a 2D analysis graph of the strain position against the back-body surface.

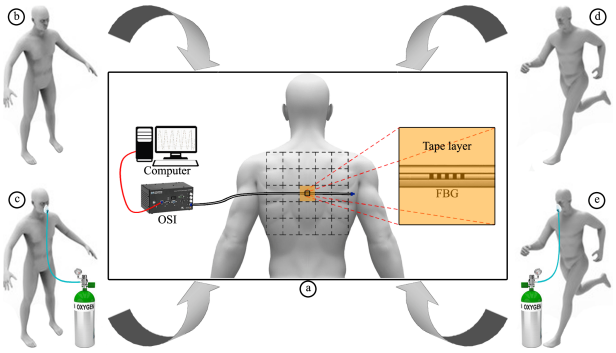

Fig. 4. Measurement of human respiratory characteristics is carried out by (a) inducing FBG through the back-body surface, where the FBG strain is connected directly to OSI and then forwarded to a computer. This experiment was tested with the object standing still while breathing (b) normally and (c) with supplemental oxygen. In addition, the object also performs running activities while breathing (d) normally and (e) administering additional oxygen.

6. FBG strains distribution

Normal breathing is maintained for 60 seconds for each object while standing still. The FBG strain profile produced for each object is shown in Fig. 5(a). The results of FBG strain measurements from the position of each object were more dominantly detected in the middle back area. Objects O1 and O3 have the same FBG strain distribution with

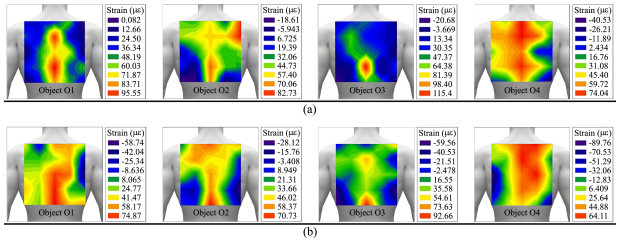

Fig. 5. FBG strain distribution on the back-body surface in the condition of the object standing still while breathing (a) normal and (b) supplemental oxygen.

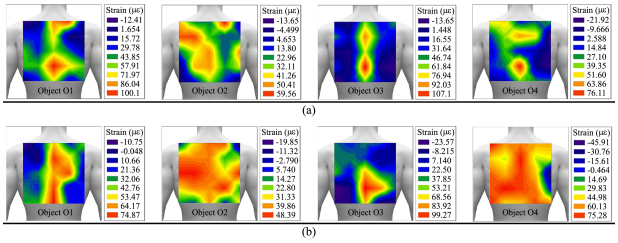

Fig. 6. FBG strain distribution on the back-body surface in the condition of the running object while breathing (a) normal and (b) supplemental oxygen.

peak values right on the slightly lower back of 95.55$\mu\varepsilon$ and 115.4$\mu\varepsilon$. Objects O 2 and O 4 also have the same profile with the highest distribution of FBG strains in the upper back of 82.73$\mu\varepsilon$ and 74.04$\mu\varepsilon$. Even so, the highest FBG strain values were obtained relatively in the middle back. These results are consistent with the reports of Dziuda et al. (2012) that the strongest physiological signals were obtained when the FBG was positioned along the longitudinal axis of the body [3].

A Comparison of FBG strains under standing still breathing conditions using oxygen flow is shown in Fig. 5(b). The addition of oxygen flow in the body by 4 l/minute is conditioned by the levels of each object as measured using an oximeter. The FBG strain distribution area for object O1 has increased by more than 70% with the highest strain value in the lower back area of 74.87$\mu\varepsilon$. Objects other than O 1 had a more distribution of FBG strains in the upper back area with an estimated mean area increase of 40%. However, the peak value of the FBG strain for objects O2 and O3 is located on the lower back with values of 70.73$\mu\varepsilon$ and 92.66$\mu\varepsilon$. At the same time, object *O*4 has a peak FBG strain of 64.11$\mu\varepsilon$ on the upper back. In that case, the increased flow of oxygen in the breath causes the back-body to stretch even more extensively. Therefore, the pressure gradient applied and the response perceived by the FBG progressively increases over a wider area. Detailed data regarding FBG strains on the back-body surface with an object standing upright can be seen in Table 3.

The FBG strain distribution for each object as shown in Fig. 6(a) is the result of measuring the condition of the object running with normal breathing. Objects O1 and O3 have exactly the same FBG strain distribution in the vertical spine with peak values of 100.1 $\mu\varepsilon$ and 107.1$\mu\varepsilon$ in the low back. Compared to objects O 2 and O 3 , the most dominant FBG strain distribution was on the upper back with values of 59.56$\mu\varepsilon$ and 76.11$\mu\varepsilon$. The resulting FBG strain appears to be increased compared to the standing state. This is because objects require more air intake when running so the FBG strain increases because the back of the body experiences a greater stretch. In addition, the spread of strain on the back varies due to the FBG response by other parameters such as circulation of air, blood, and other fluids, including body movements. The spread of strain that occurs in these three objects is very small due to the work of the body's metabolism and also the temperature after activity [36]. However, the resulting strain is still concentrated in the vertical region of the back.

Fig. 6(b) is the FBG strain distribution for each object in running conditions while breathing using supplemental oxygen. The addition of an oxygen flow of 4 l/min aims to determine the body's response to the distribution of strain that occurs on the back of each object. Furthermore, the FBG strain distribution varies more when the activity is carried out because the pressure of human motion changes. This results in changes in human body temperature at the time of sampling. Objects O1 and O3 experienced a smaller increase in the distribution area of the FBG strain by 20% with the highest values being 74.97$\mu\varepsilon$ and 99.27$\mu\varepsilon$ on the lower back. However, objects O 2 and O4 experienced a remarkable increase in the FBG strain distribution of 90% with the highest values being in the mid-back of 48.39$\mu\varepsilon$ and 75.28$\mu\varepsilon$. Strain distribution occurs in each object when carrying out activities that are larger and more frequent than other measurement conditions. The strain value varies because the body's response to activity requires more oxygen intake to 75 times per minute. On the other hand, it requires 12 to 20 times per minute under normal conditions. Therefore, the faster a person breathes, the more strain occurs. Complete detailed data regarding the FBG strain on the back surface of the body with a running object can be seen in Table 4.

7. Conclusions

This study successfully designed and measured FBG on nasal respiratory flow, as well as the response on the back-body surface. FBG produces a wavelength function strain

Table 3. FBG strain on the back-body surface with the object standing upright

Object	Value	FBG strain ($\mu\varepsilon$)	
		Normal	Supplemental oxygen
O1	Max	95.55	74.87
	Min	0.082	-58.74
O2	Max	82.73	70.73
	Min	-18.61	-28.12
O3	Max	115.4	92.66
	Min	-20.68	-59.56
O4	Max	74.04	64.11
	Min	-40.53	-89.76

Table 4. FBG strain on the back-body surface with running object

Object	Value	FBG strain (μs)	
		Normal	Supplemental oxygen
O1	Max	100.1	74.87
	Min	-12.41	-10.75
O2	Max	59.56	48.39
	Min	-13.65	-19.85
O3	Max	107.1	99.27
	Min	-13.65	-23.57
O4	Max	76.11	75.28
	Min	-21.92	-45.91

value on the order of 10^{-6} in normal breathing conditions with additional oxygen flow. In this case, the largest strain was at the top and middle positions of the mask. The strain value decreases with the addition of oxygen flow due to stress. Furthermore, the oxygen levels increase with the addition of external oxygen flow. For designs and measurements at the mid-back position that occurs vertically, the most frequently in a rather central position. The condition of objects that are active using oxygen flow gives more stretch responses. This is influenced by several internal factors, such as weight, genetics, and neglected hormonal disorders. However, this FBG system has the advantage of measuring respiration in terms of subtle strain factors in an emergency call for the development of a human respiratory FBG sensor.

Acknowledgements

The authors expressed profound gratitude to the Ministry of Education and Culture of the Indonesian Government and Universitas Riau, Pekanbaru, for providing financial support and grant through the Lembaga Penelitian dan Pengabdian Kepada Masyarakat (Research Institution and Community Services) Universitas Riau, 2024.

References

[1] W.-H. Shi, W.-M. Lv, T.-Y. Sun, and B.-S. Zhang, (2019) *"Optoelectronic platform and technology"* **Frontiers of Information Technology and Electronic Engineering *20***: 439–457. DOI: 10.1631/FITEE.1800451.

[2] D. Tosi, E. Schena, C. Molardi, and S. Korganbayev, (2018) *"Fiber optic sensors for sub-centimeter spatially resolved measurements: Review and biomedical applications"* **Optical Fiber Technology *43***: 6–19. DOI: 10.1016/j.yofte.2018.03.007.

[3] L. Dziuda, J. Lewandowski, F. Skibniewski, and G. Nowicki, (2012) *"Fibre-optic sensor for respiration and heart rate monitoring in the MRI environment"* **Procedia Engineering *47***: 1291–1294. DOI: 10.1016/j.proeng.2012.09.391.

[4] A. Leal-Junior, C. Marques, and A. Frizera, (2022) *"Diaphragm-assisted impact amplitude and localization measurement system with FBG sensors"* **Optical Fiber Technology *70***: 102854. DOI: 10.1016/j.yofte.2022.102854.

[5] J. Yu, C. Li, X. Qiu, and H. Chen, (2021) *"A full-optical strain FBG sensor for in-situ monitoring of fatigue stages via tunable DFB laser demodulation"* **Optical and Quantum Electronics *53***: 1–12. DOI: 10.1007/s11082-021-02800-7.

[6] P. Hariprasad, C. Chanchal, P. Anita, G. Arun, and S. Sandeep, (2023) *"Development of a prototype fiber-optic biosensor for the detection of lipase inhibitors"* **Kuwait Journal of Science *50***: 333–338. DOI: 10.1016/j.kjs.2023.05.009.

[7] T. Saktioto, F. D. Fadilla, Y. Soerbakti, and D. Irawan, (2021) *"Application of fiber Bragg grating sensor system for simulation detection of the heart rate"* **Journal of Physics: Conference Series *2049***: 012002. DOI: 10.1088/1742-6596/2049/1/012002.

[8] H. Z. Yang, S. W. Harun, and H. Ahmad, (2011) *"Theoretical and experimental studies on concave mirror-based fiber optic displacement sensor"* **Sensor Review *31***: 65–69. DOI: 10.1108/02602281111099107.

[9] C. Hong, Y. Yuan, Y. Yang, Y. Zhang, and Z. A. Abro, (2019) *"A simple FBG pressure sensor fabricated using fused deposition modelling process"* **Sensors and Actuators A: Physical *285***: 269–274. DOI: 10.1016/j.sna.2018.11.024.

[10] C. Hong, Y. Zhang, and L. Borana, (2019) *"Design, fabrication and testing of a 3D printed FBG pressure sensor"* **IEEE Access *7***: 38577–38583. DOI: 10.1109/ACCESS.2019.2905349.

[11] N. A. Rosman, C. B. M. Rashidi, S. A. Aljunid, and R. Endut, (2020) *"Temperature monitoring system using fiber Bragg grating (FBG) approach"* **AIP Conference Proceedings *2203***: 020065. DOI: 10.1063/1.5142157.

[12] X. Wang, Y. Jiang, S. Xu, H. Liu, and X. Li, (2022) *"Fiber Bragg grating-based smart garment for monitoring human body temperature"* **Sensors *22***: 4252. DOI: 10.3390/s22114252.

[13] T. Saktioto, Y. Soerbakti, A. Thoibah, B. Meyzia, R. F. Syahputra, D. Irawan, and H. Hairi, (2023) *"Numerical investigation of physical parameters in cardiac vessels as a new medical support science for complex blood flow characteristics"* **Baghdad Science Journal *20***: 2322–2329. DOI: 10.21123/bsj.2023.7076.

[14] Defrianto, T. Saktioto, N. Hikma, Y. Soerbakti, D. Irawan, Okfalisa, B. Widiyatmoko, and D. Hanto, (2022) *"External perspective of lung airflow model through diaphragm breathing sensor using fiber optic elastic belt"* **Indian Journal of Pure and Applied Physics *60***: 561–566. DOI: 10.56042/ijpap.v60i7.62342.

[15] S. Saktioto, D. Defrianto, A. Thoibah, Y. Soerbakti, R. F. Syahputra, S. Syamsudhuha, D. Irawan, H. Hairi, O. Okfalisa, and R. Amelia, (2023) *"Simplified kinetic model of heart pressure for human dynamical blood flow"* **Indonesian Journal of Electrical Engineering and Informatics *11***: 870–882. DOI: 10.52549/ijeei.v11i3.3473.

[16] T. Saktioto, D. Defrianto, N. Hikma, Y. Soerbakti, S. Syamsudhuha, D. Irawan, O. Okfalisa, B. Widiyatmoko, and D. Hanto, (2022) *"Airflow vibration of diaphragmatic breathing: model and demonstration using optical biosensor"* **Telkomnika (Telecommunication Computing Electronics and Control) *21***: 667–674. DOI: 10.12928/TELKOMNIKA.v21i3.23613.

[17] N. Hikma, T. Saktioto, and Y. Soerbakti, (2023) *"Vibration analysis of diaphragmatic breathing activity using single-mode fiber and fiber Bragg grating"* **AIP Conference Proceedings *2858***: 080001. DOI: 10.1063/5.0163142.

[18] H. A. Mohammed and M. H. Yaacob, (2020) *"A novel modified fiber Bragg grating (FBG) based ammonia sensor coated with polyaniline/graphite nanofibers nanocomposites"* **Optical Fiber Technology *58***: 102282. DOI: 10.1016/j.yofte.2020.102282.

[19] Z. Ruan, L. Pei, T. Ning, J. Wang, J. Wang, J. Li, Y. Xie, Q. Zhao, and J. Zheng, (2021) *"Simple structure of tapered FBG filled with magnetic fluid to realize magnetic field sensor"* **Optical Fiber Technology *67***: 102698. DOI: 10.1016/j.yofte.2021.102698.

[20] C. Cui, L. Gao, N. Dai, and Q. Xu, (2021) *"Fiber Bragg grating inclinometer-enabled IoT sensing system with low power consumption and small size"* **Sensors and Materials *33***: 2321–2331. DOI: 10.18494/SAM.2021.3281.

[21] X. Li, Y. Yang, W. Zhang, Z. Wang, Y. Yuan, H. Hu, and D. Xu, (2021) *"An FBG pressure sensor based on spring-diaphragm elastic structure for ultimate pressure detection"* **IEEE Sensors Journal *22***: 2213–2220. DOI: 10.1109/JSEN.2021.3136212.

[22] Y. He, Q. Yang, S. Sun, M. Luo, R. Liu, and G.-D. Peng, (2020) *"A multi-point voltage sensing system based on PZT and FBG"* **International Journal of Electrical Power and Energy Systems *117***: 105607. DOI: 10.1016/j.ijepes.2019.105607.

[23] J. K. Sahota, N. Gupta, and D. Dhawan, (2020) *"Fiber Bragg grating sensors for monitoring of physical parameters: A comprehensive review"* **Optical Engineering *59***: 060901. DOI: 10.1117/1.oe.59.6.060901.

[24] C. Tavares, C. Leitão, D. L. Presti, M. F. Domingues, N. Alberto, H. Silva, and P. Antunes, (2022) *"Respiratory and heart rate monitoring using an FBG 3D-printed wearable system"* **Biomedical Optics Express *13***: 2299–2311. DOI: 10.1364/boe.452115.

[25] M. Filosa, L. Massari, D. Ferraro, G. D'Alesio, J. D'Abbraccio, A. Aliperta, D. L. Presti, J. D. Tocco, M. Zaltieri, C. Massaroni, M. C. Carrozza, M. Ferrarin, M. D. Rienzo, E. Schena, and C. M. Oddo, (2022) *"A meta-learning algorithm for respiratory flow prediction from FBG-based wearables in unrestrained conditions"* **Artificial Intelligence in Medicine *130***: 102328. DOI: 10.1016/j.artmed.2022.102328.

[26] W. Chen, J. Wang, F. Wan, and P. Wang, (2019) *"Review of optical fibre sensors for electrical equipment characteristic state parameters detection"* **High Voltage *4***: 271–281. DOI: 10.1049/hve.2019.0157.

[27] V. Mishra, N. Singh, U. Tiwari, and P. Kapur, (2011) *"Fiber grating sensors in medicine: Current and emerging applications"* **Sensors and Actuators A: Physical *167***: 279–290. DOI: 10.1016/j.sna.2011.02.045.

[28] C. E. Campanella, A. Cuccovillo, C. Campanella, A. Yurt, and V. M. N. Passaro, (2018) *"Fibre Bragg grating based strain sensors: Review of technology and applications"* **Sensors *18***: 3115. DOI: 10.3390/s18093115.

[29] R. Li, Y. Chen, Y. Tan, Z. Zhou, T. Li, and J. Mao, (2018) *"Sensitivity enhancement of FBG-based strain sensor"* **Sensors *18***: 1607. DOI: 10.3390/s18051607.

[30] M. S. Siobal, (2016) *"Monitoring exhaled carbon dioxide"* **Respiratory Care *61***: 1397–1416. DOI: 10.4187/respcare.04919.

[31] A. Issatayeva, A. Beisenova, D. Tosi, and C. Molardi, (2021) *"Fiber-optic based wearables for the continuous monitoring of respiratory rate"* **Biophotonics in Exercise Science, Sports Medicine, Health Monitoring Technologies, and Wearables II *11638***: 1163805. DOI: 10.1117/12.2582461.

[32] C. Shi, Z. Tang, H. Zhang, and Y. Liu, (2023) *"Development of an FBG-based wearable sensor for simultaneous respiration and heartbeat measurement"* **IEEE Transactions on Instrumentation and Measurement *72***: 1–9. DOI: 10.1109/TIM.2022.3228276.

[33] J. Zhang, Z. Lian, Z. Zhou, Z. Song, M. Liu, and K. Yang, (2022) *"Leakage detection in a buried gas pipeline based on distributed optical fiber time-domain acoustic wave signal"* **Engineering Failure Analysis *141***: 106594. DOI: 10.1016/j.engfailanal.2022.106594.

[34] J. Gómez, J. R. Casas, and S. Villalba, (2020) *"Structural health monitoring with distributed optical fiber sensors of tunnel lining affected by nearby construction activity"* **Automation in Construction *117***: 103261. DOI: 10.1016/j.autcon.2020.103261.

[35] H. Merdji, A. Curtiaud, A. Aheto, A. Studer, V.-P. Harjola, A. Monnier, K. Duarte, N. Girerd, M. Kibler, H. Ait-Oufella, J. Helms, A. Mebazaa, B. Levy, A. Kimmoun, and F. Meziani, (2022) *"Performance of early capillary refill time measurement on outcomes in cardiogenic shock: An observational, prospective multicentric study"* **American Journal of Respiratory and Critical Care Medicine *206***: 1230–1238. DOI: 10.1164/rccm.202204-0687OC.

[36] R. Min, X. Hu, L. Pereira, S. Soares, L. C. B. Silva, G. Wang, L. Martins, H. Qu, P. Antunes, C. Marques, and X. Li, (2022) *"Polymer optical fiber for monitoring human physiological and body function: A comprehensive review on mechanisms, materials, and applications"* **Optics and Laser Technology *147***: 107626. DOI: 10.1016/j.optlastec.2021.107626.